

Measurement of inter and intra fraction organ motion in radiotherapy using cone-beam CT projection images

T E Marchant, A M Amer¹ and C J Moore

North Western Medical Physics, Christie Hospital NHS Foundation Trust, Manchester, M20 4BX, UK.

Abstract. A method is presented for extraction of intra and inter fraction motion of seeds/markers within the patient from cone beam CT (CBCT) projection images. The position of the marker is determined on each projection image and fitted to a function describing the projection of a fixed point onto the imaging panel at different gantry angles. The fitted parameters provide the mean marker position with respect to the isocentre. Differences between the theoretical function and the actual projected marker positions are used to estimate the range of intra fraction motion and the principal motion axis in the transverse plane. The method was validated using CBCT projection images of a static marker at known locations and of a marker moving with known amplitude. The mean difference between actual and measured motion range was less than 1 mm in all directions, although errors of up to 5 mm were observed when large amplitude motion was present in an orthogonal direction. In these cases it was possible to calculate the range of motion magnitudes consistent with the observed marker trajectory. The method was shown to be feasible using clinical CBCT projections of a pancreas cancer patient.

This is an author-created, un-copyedited version of an article accepted for publication in Physics in Medicine and Biology. IOP Publishing Ltd is not responsible for any errors or omissions in this version of the manuscript or any version derived from it. The definitive publisher-authenticated version is available online at <http://dx.doi.org/10.1088/0031-9155/53/4/018>.

¹ Current institution: African Oncology Institute, Sabratha, Libya.

Introduction

In recent years, linear accelerators with integrated cone beam (CB) CT became available and now provide volumetric imaging of the patient in the treatment position (Jaffray *et al.*, 2002; McBain *et al.*, 2006). CBCT images can be used to measure inter-fraction set-up error through matching of bony structures to the planning CT scan (Oldham *et al.*, 2005). For some disease sites, CBCT image quality is sufficient for soft tissue matching of target organs, allowing corrections for inter-fraction organ motion to be made (Smitsmans *et al.*, 2005). However, 3D CBCT is a static image and does not give dynamic information on the intra-fraction motion taking place during treatment. Information about intra *and* inter fraction target motion is required for treatment planning in order to determine the appropriate margin that should be used to grow the clinical target volume into the planning target volume. Respiratory motion may be measured before treatment, for example using 4D CT, and a model of the motion constructed for use during treatment planning (Low *et al.*, 2005). Patient-specific motion models may also be used to compensate motion and improve image quality of CBCT imaging in the presence of respiratory motion (Li *et al.*, 2006). Pre-treatment motion measurements may not remain valid over the course of treatment, and verification during treatment may be required. For lung this problem has been addressed through the development of respiratory correlated 4D CBCT (Sonke *et al.*, 2005), however this approach requires increased numbers of projection images (with correspondingly increased imaging dose) and relies on the assumption of periodic motion. Alternatively, fluoroscopy systems have been used for real-time tumour tracking using implanted markers during radiotherapy delivery (Shirato *et al.*, 2006).

CBCT projection images consist of at least thirty seconds of rotational fluoroscopic images per half-scan for integrated image guided treatment machines, since the maximum gantry scanning speed is limited to 7°/s according to IEC standards (IEC, 1998). Dynamic information is contained in the projections when a CBCT scan is acquired, although the projection data is often discarded once volumetric reconstruction has taken place. The purpose of this study is to show that the projection images can be used to extract dynamic information about organ position, specifically to measure intra as well as inter fraction variability. In order to track motion from CBCT projection images, it is necessary to be able to detect the tissue or organ of interest. Soft tissue organs are usually not clearly visible in projection images, so this study uses surrogate markers, implanted into or near the target site. Markers are readily visible on the projection images because of the kV energy spectrum of the imaging source (Sorcini and Tilikidis, 2006).

1. Materials and Methods

1.1. Cone beam CT projection images

CBCT images were acquired using an Elekta Synergy™ integrated image guided treatment machine (Elekta Systems, Crawley, UK), shown in Figure 1a. This system has a kV imager fixed to the rotating gantry, mounted orthogonally to the MV treatment beam. The kV imager fires horizontally when the gantry angle is zero degrees. Projection images were captured over 360° of rotation at a frame rate of 5.5Hz, with approximately 660 projections per scan, i.e. a total scanning time of 120 seconds. Projection images were acquired using a 512x512 matrix with pixel size 0.8 mm at the detector.

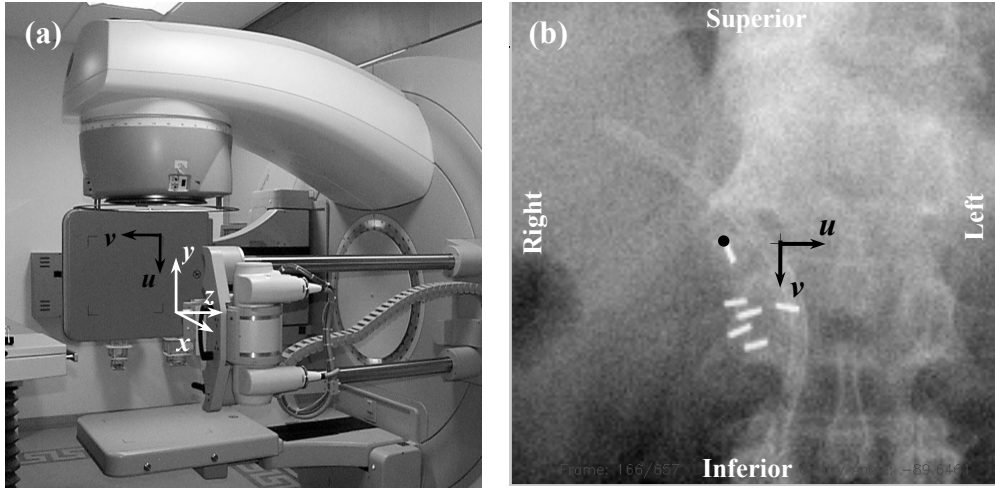


Figure 1. (a) Linear accelerator with CBCT system with room coordinates (x, y, z) indicated in white and imaging panel coordinates (u, v) in black (b) Typical projection image of pancreas patient showing visible markers and stent. The black circle indicates a manually marked point placed at the edge of one of the marker seeds.

1.2. Determination of marker position

The projection of a 3D point $P(x, y, z)$ onto a 2D plane (the amorphous silicon flat panel detector) rotating about the z axis through the volume of interest containing P can be determined by first finding the x' , y' and z' components in the rotating frame of reference, shown in Figure 2. The room coordinate system used here defines x , y and z as the conventional lateral, vertical and longitudinal directions respectively (see Figure 1a). Note that the z -axis coincides with the axis of rotation of the imaging system, rather than the vertical direction as in the IEC standard for radiotherapy equipment (IEC, 1996). Rotation of the kV imaging system about the z -axis by angle θ from the horizontal produces a set of transformed coordinates (x', y', z') related to the room coordinates (x, y, z) by;

$$\begin{pmatrix} x' \\ y' \\ z' \end{pmatrix} = \begin{pmatrix} \cos \theta & -\sin \theta & 0 \\ \sin \theta & \cos \theta & 0 \\ 0 & 0 & 1 \end{pmatrix} \begin{pmatrix} x \\ y \\ z \end{pmatrix}, \quad (1)$$

where the direction of rotation, θ , is defined as positive for clockwise rotation of the gantry. Unless on the z -axis itself, rotation alters the distance of a point from a correspondingly rotated 2D projection plane. Hence, the components of a point are differentially magnified when projected to form tangential and axial coordinates u and v on the imaging panel, Figure 2.

$$u(\theta) = y' \times \frac{SDD}{(SAD - x')} \quad (2)$$

$$v(\theta) = z' \times \frac{SDD}{(SAD - x')} \quad (3)$$

Magnification depends on SDD and SAD , which are the distances from the source to the detector and axis of rotation respectively. For the linac mounted CBCT system used here, $SDD = 1536$ mm and $SAD = 1000$ mm.

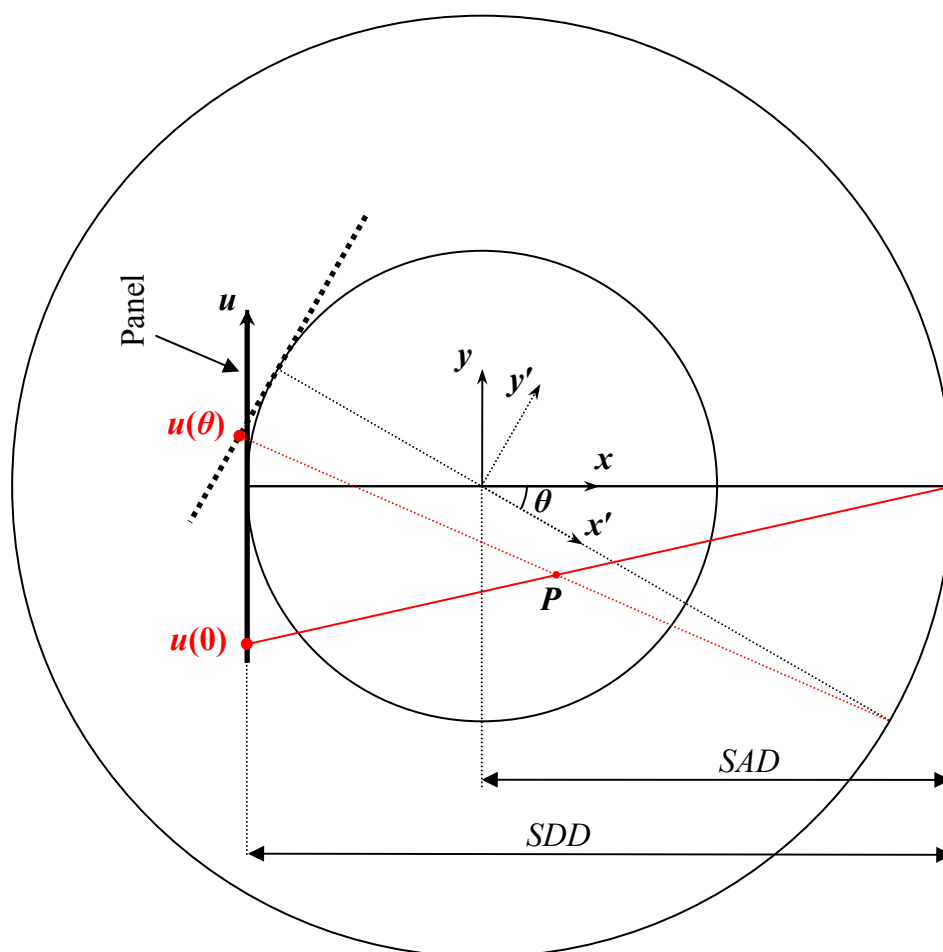


Figure 2. Geometry of cone beam CT system.

In this study, the end position of a seed/stent was determined manually on each projection image giving $P(u, v)$. An example projection image showing a manually placed seed end point is shown in Figure 1b. The resulting u and v positions as a function of gantry angle were then fitted to the above rotational functions giving the mean seed position $(\bar{x}, \bar{y}, \bar{z})$ on that fraction with respect to the isocentre. The robustness of the fitting procedure in the presence of periodic respiratory motion was improved by boxcar smoothing of marked u and v positions in time over approximately 5 seconds, typically covering at least one breathing cycle.

Note that it is not possible to derive the exact marker position (x, y, z) in 3D space on each projection from the measured (u, v) data since one of the axes, x' , is not measured. Only the mean marker position was found using the fitted data.

1.3. Inter and intra fraction motion

Inter fraction organ motion with respect to the first day was determined from the mean positions while the differences between the mean and actual seed positions in each projection represent the intra fraction motion.

Intra-fraction motion in the x and y directions was estimated from the difference between the actual seed u position and the expected u of the mean seed position, scaled back to the seed location in real space (i.e. the magnification is corrected using the estimated mean x, y position

of the marker). The range of these differences on a series of projection images was used as a measure of the magnitude (i.e. peak-to-peak range) of the intra-fraction motion.

Only projection images acquired around gantry angles 90° and -90° ($\pm 10^\circ$) i.e. $|80^\circ-100^\circ|$, were used to extract intra-fraction motion in the x direction to minimize the effect of motion in the y direction (note that the kV imager is orthogonal to the gantry angle) These directions maximize transverse movement and minimize the effect of in-line (i.e. vertical) motion uncertainties. The use of 20 degrees of projection images is typically sufficient to capture a full breathing cycle since it equates to 6-7 seconds. Calculation of motion in the y direction was restricted to projection images from $(-180^\circ$ to $-160^\circ)$, $(-10^\circ$ to $10^\circ)$ and $(160^\circ$ to $180^\circ)$ for similar reasons. For a full rotation CBCT acquisition, these ranges include the first and last 20° of the rotation, thus including a larger angular range around 180° ($\pm 20^\circ$). This is necessary because the $\pm 10^\circ$ range is not acquired as a continuous sequence of projections. For intra fraction motion in the z direction, the difference in the v direction was used for all projection images.

If only projections from the lateral (AP) direction were used to determine the AP (lateral) seed motion then there would be only a small error, due to changes in magnification with seed position in the source-detector direction ($\sim 1\%$ per cm). Projections taken from a range of angles around the orthogonal projection are used to determine seed motion, but are treated as if they were taken from the orthogonal direction. This leads to an additional error, which increases with the angle from the orthogonal direction. The magnitude of this error can be predicted given the known mean seed position and the magnitude of motion observed. This was done empirically at each projection angle by simulating the projected coordinate of all possible marker positions consistent with the observed mean position and motion. The error was then calculated as the maximum difference between the observed and actual marker position over all simulated positions. This value indicates the maximum expected error for a measurement at that gantry angle. The error ranges up to approximately 20% of the magnitude of the motion in the direction orthogonal to that being measured at 10° from the projection angle orthogonal to the motion direction being measured. The predicted errors were used to quote a range about the measured motion magnitude, the size of which indicates the uncertainty of the measurement. This was done by finding the maximum and minimum motion magnitude that was consistent with the predicted errors in marker position.

1.4. Validation of marker position and motion measurements

The determination of marker position and motion range based on CBCT projection images was validated using images of a spherical glass bead (3mm diameter) placed at known positions relative to the isocentre. CBCT projection images were acquired with the bead aligned with the isocentric lasers and also offset by known distances in the three orthogonal directions (x,y,z) (see Table 1). The uncertainty in the positioning of the marker bead was estimated to be $\pm 0.5\text{mm}$ (SD) due to the precision of manual alignment to the isocentric lasers, and of shifts to the marker position applied using the couch readouts. The bead was then attached to a motor allowing periodic circular motions of different magnitudes and in different orientations to be applied (see Table 1). The applied motion magnitude was found by measuring the distance of the marker from the axis of its rotation with an estimated uncertainty of $\pm 0.5\text{mm}$. The frequency of the periodic motion was approximately 14 rpm. The projection images were analysed by marking the centre of the bead in each projection and calculating the mean position and range of motion in each direction using the method described in sections 2.2-2.3. The measured and known mean positions and motion ranges were compared.

1.5. Application to clinical images

The method was also tested for clinical data using projections from a CBCT image of a pancreatic cancer patient to determine pancreas motion. The patient had gold seeds (1mm x

10mm) placed into the pancreas at attempted surgery. The position of one end of a seed was marked manually in each projection image, and the mean position and range of motion of the seed was calculated using the methods described above.

1.6. Detection of principal motion axes

In addition to the tumour motion magnitudes in each direction, it is also possible to determine the principal axes of motion from the CBCT projection images, at least in the transverse plane. The difference between the projected marker u position and the fitted mean position is plotted as a function of gantry angle. The result will be an oscillating function with maximum amplitude at a certain angle. The projection direction at maximum amplitude will be orthogonal to the major axis of motion in the transverse plane. Determination of the principal motion axis in the transverse plane was demonstrated using the test data of a marker moving with known amplitude in the y - z plane, and also with the patient CBCT image.

1.7. Precision of manual marker detection

In this study, the identification of marker positions in the projection images was done by the manual placing of points. A marker was identified four times on all 660 projections of one of the CBCT scans by an expert clinical observer. The precision of manual marker identification was investigated by measuring the differences between the repeated u and v positions identified and the mean of the four measurements.

It was found that the gold markers were clearly visible in all of the clinical projection images, making identification of marker position a simple task. The standard deviations of the difference between each repeated measurement of marker position and the mean of the four measurements are 0.3mm and 0.2mm in the u and v directions respectively measured at the imaging panel.

2. Results

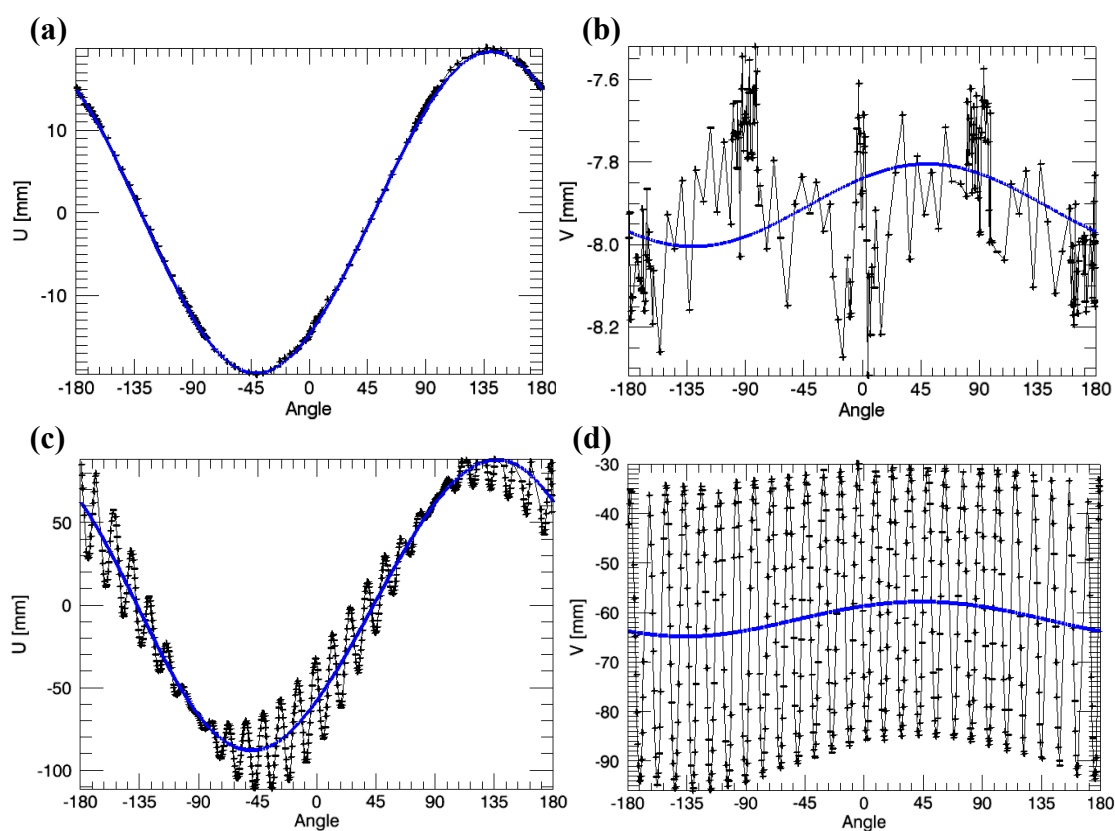
2.1. Validation of marker position and motion measurements

Table 1 shows the actual and measured values of mean marker position and motion magnitude in each direction (note that motion magnitude is displayed as full peak-to-peak range). Figure 3(a-b) shows the u and v positions as a function of gantry angle for a static marker offset from the isocentre by -7 mm, 9 mm and 5 mm in the x , y and z directions respectively (image 2 in Table 1). Figure 3(c-d) shows the u and v positions as a function of gantry angle for a marker moving with magnitude 0 mm, 40 mm and 40 mm in the x , y and z directions respectively, whose mean position is offset from the isocentre by -40 mm, 40 mm and 40 mm in the x , y and z directions respectively (image 9 in Table 1).

Figure 4(a-c) shows the data used to determine the motion magnitude in each direction for the static marker. Figure 4(d-f) shows the data used to determine the motion magnitude in each direction for the dynamic marker. The plots show the difference between the measured marker coordinate and the expected coordinate for a static marker at the fitted mean (i.e. the difference between the data points and fitted function in Figure 3). A magnification correction is included to account for the difference in scale between the imaging panel and the isocentre. The plots are displayed as a function of time rather than gantry angle to indicate the marker motion. The error bars indicate the potential error due to the oblique projection angle, as described in section 2.3. The motion magnitude, shown above each plot is defined as the maximum difference minus the minimum difference. Values in square brackets indicate the maximum and minimum motion magnitude that is consistent with the predicted errors on the observed data taking into account the angular range of projection data used.

Table 1. Comparison of known and measured mean marker position and motion magnitude (peak to peak).

Img	Actual (mm)						Measured (mm)					
	Mean			Magnitude			Mean			Magnitude		
#	<i>x</i>	<i>y</i>	<i>z</i>	<i>x</i>	<i>y</i>	<i>z</i>	<i>x</i>	<i>y</i>	<i>z</i>	<i>x</i>	<i>y</i>	<i>z</i>
1	0	0	0	0	0	0	-1	1	0	0	0	0
2	-7	9	5	0	0	0	-8	10	5	0	1	1
3	-60	70	50	0	0	0	-62	69	51	0	0	1
4	0	0	0	10	10	0	0	0	0	9	10	1
5	0	0	0	0	10	10	-1	1	0	-	-	10
6	0	0	0	40	40	0	0	1	0	38	39	1
7	0	0	0	0	40	40	0	1	0	5	38	38
8	-40	40	40	40	40	0	-39	38	41	40	38	2
9	-40	40	40	0	40	40	-42	40	40	5	38	40

**Figure 3.** Validation test of mean marker position measurements. Points show measured positions and thick curve shows fitted values. (a) *u* position (b) *v* position as a function of gantry angle for static marker at (*x,y,z*) position (-7, 9, 5) mm. (c) *u* position (b) *v* position for marker at (*x,y,z*) mean position (-40, 40, 40) mm moving with range 0mm, 40mm and 40mm in the *x,y*, and *z* directions respectively.

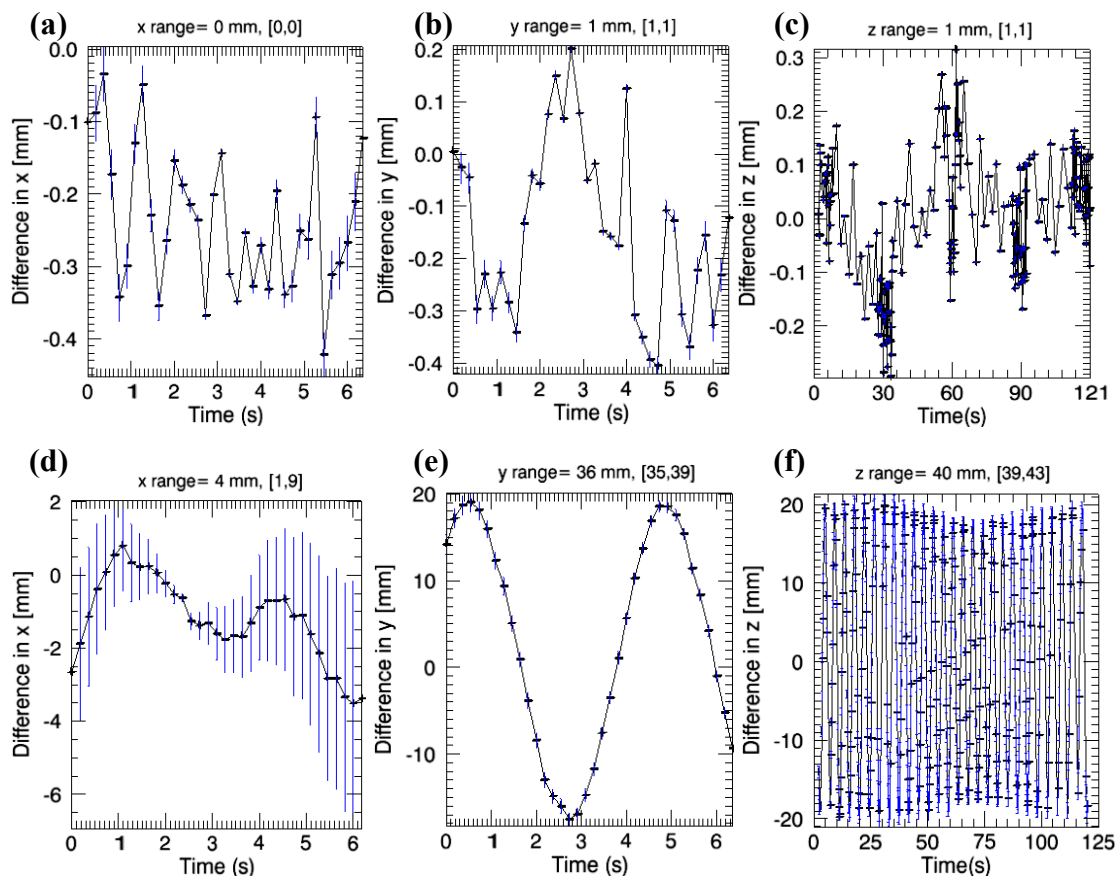


Figure 4. Validation of motion magnitude measurements. Measured motion in (a) lateral ($80^\circ < \theta < 100^\circ$) (b) vertical ($-10^\circ < \theta < 10^\circ$) and (c) longitudinal ($-180^\circ < \theta < 180^\circ$) direction for static marker. Measured motion in (d) lateral ($80^\circ < \theta < 100^\circ$) (e) vertical ($-10^\circ < \theta < 10^\circ$) and (f) longitudinal ($-180^\circ < \theta < 180^\circ$) direction for marker moving with range 0mm, 40mm, 40mm in the x , y and z directions respectively. Motion magnitude (range) is shown above the plot. Figures in square brackets give the minimum and maximum range that is consistent with the estimated error bars plotted.

The mean (SD) of the difference between actual and measured mean marker position over all test images was 0.7 (1.0), 0.2 (1.1), and 0.2 (0.4) mm in the lateral, vertical and longitudinal directions respectively. The maximum difference between the known and measured marker position was 2mm. Mean marker position measurements were still reliable even when large magnitude motion was applied.

Measurements of motion magnitude also showed no significant error for the static markers (mean error was less than 1mm for all directions), however some errors of up to 5mm were observed in cases where large magnitude motion was present. This was due to the use of a range of angles about the cardinal angles causing displacement in one direction to be attributed to the orthogonal direction. The estimated uncertainty on the measured range of motion (indicated by the error bars and ranges in square brackets shown in Figure 4) proved to be a good indication of the true error.

In one case measurements of lateral and vertical motion magnitude could not be made because the marker bead was not visible in a sufficient number of projections from the necessary gantry angles (image 5 in table 1). This is because it was masked by high density structures in the couch and the motor used to generate the motion.

2.2. Application to clinical images

Figure 5 shows the u and v positions of the seed as a function of gantry angle marked for the clinical images of the pancreas patient. The mean position of the seed was determined relative to the isocentre to be -6mm , 4mm and 4mm in the x , y and z directions respectively. Figure 6 shows the range of motion of the seed measured in the clinical images in each direction. The range was measured to be 1mm , 3mm and 11mm in the x , y , and z directions respectively. The largest range of pancreatic motion was measured in the z (longitudinal) direction. This is as expected due to respiratory motion of the diaphragm.

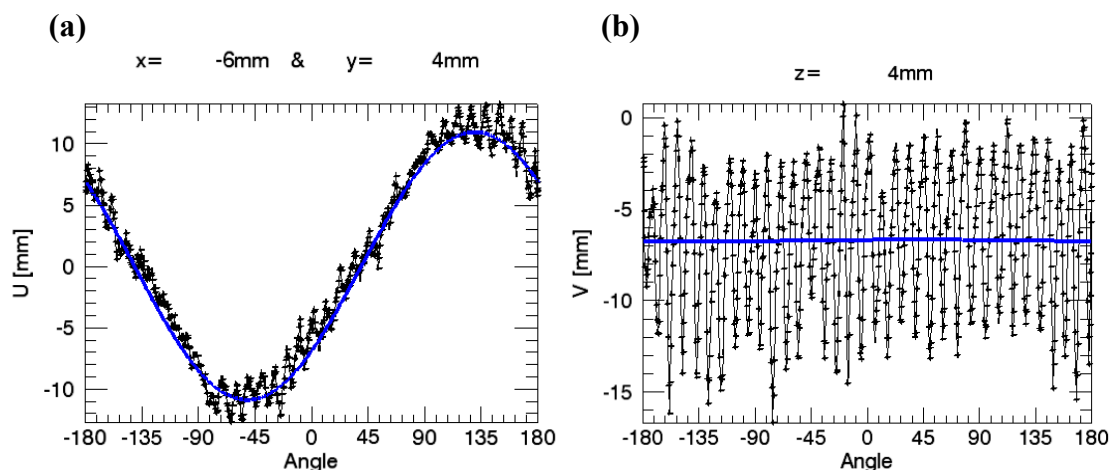


Figure 5. Pancreas patient image: (a) u position of seed as a function of gantry angle (points) with theoretical function for an object located at $x=-6\text{mm}$ and $y=4\text{mm}$ overlaid (thick line) (b) v position of seed as a function of gantry angle (points) with theoretical function for object located at $z=4\text{mm}$ overlaid (thick line).

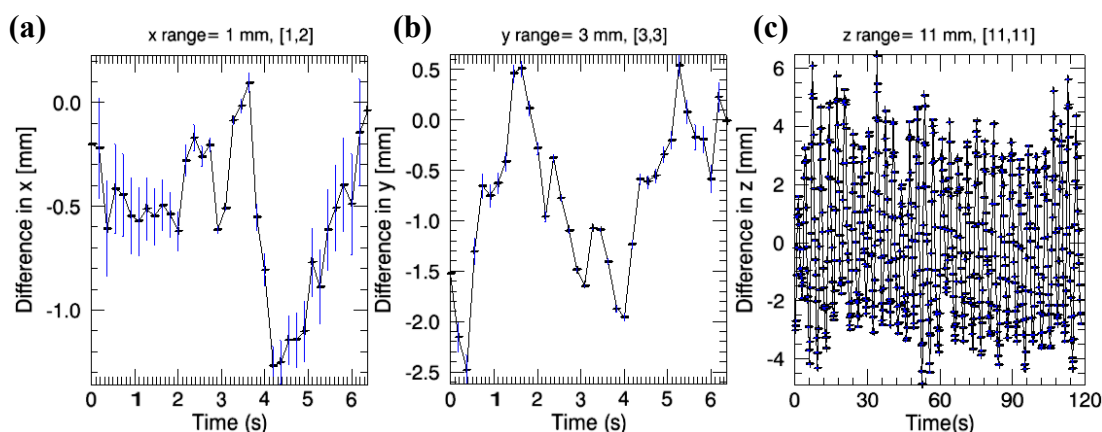


Figure 6. Pancreas patient image: Measured intra-fraction motion in (a) x (LR) direction ($80^\circ < \theta < 100^\circ$) (b) y (AP) direction ($-10^\circ < \theta < 10^\circ$) (c) z (CC) direction ($-180^\circ < \theta < 180^\circ$). Error bars represent expected error due to orthogonal seed motion. The uncertainty in manual seed identification (approximately 0.5mm) is not included. Figures in square brackets give the minimum and maximum range that is consistent with the estimated error bars plotted.

2.3. Detection of principal motion axes

Figure 7a shows the data used to determine the principal motion axis in the transverse plane for the test marker moving with magnitude 40mm in the y and z directions and with (x,y,z) mean position $(-40, 40, 40)$ mm. This figure shows the difference between the measured marker positions and the fitted curve shown in figure 3c. The maximum amplitude of

oscillation occurs close to gantry angle 0° and 180° . This corresponds to a projection angle along the x -axis, indicating the principal axis of motion in the transverse plane is along the y -axis. This is as expected for a marker moving only in the y and z directions. There are some data points missing from figure 7a, corresponding to projections where the marker could not be identified due to occlusion by high density objects in the motor used to apply the motion. Angular ranges containing missing data points are indicated by grey shading in the figure.

Figure 7b shows the data used to determine the principal motion axis in the transverse plane for the patient CBCT image. The modulation of oscillation amplitude with gantry angle is not as clear as for the test data because of the smaller motion amplitude and less regular motion pattern. However, the maximum amplitude was measured to occur at approximately -20° and 160° . This corresponds to a principal motion axis angled at approximately 20° to the AP axis.

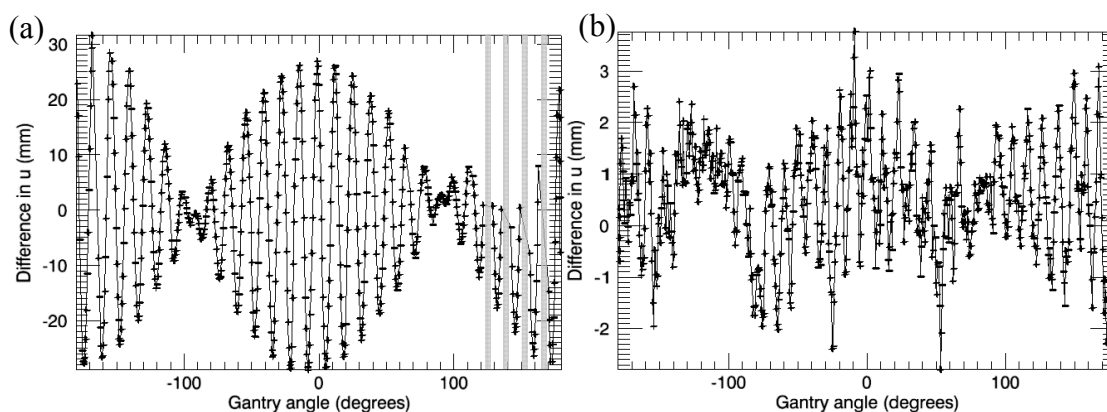


Figure 7. Difference between u -position of marker and fitted ideal curve as a function of gantry angle for (a) test phantom data (b) patient data. Angular ranges shaded grey indicate regions of missing data.

3. Discussion

The results given above show that the mean position and motion magnitude of a static or cyclically moving marker can be measured from a sequence of CBCT projection images. The error on the mean marker position was 1mm (SD) or less with no significant systematic error. Small differences (of approximately 1mm or less) between the actual and measured mean marker position are within the expected precision of the marker alignment as discussed in section 2.4.

This study used manual marker identification from the projection images. This was found to be possible due to the good visibility of gold seeds in the projection images, although the time taken was significant at up to 30 minutes for a complete set of 650 projection images. The positional uncertainty due to manual marker identification was acceptably small at around 0.5mm (1 SD). It is likely that this uncertainty could be reduced using automatic marker detection techniques such as those used previously for megavoltage portal images (Sykes *et al.*, 2003) and kilovoltage marker tracking (Shirato *et al.*, 2000; Tang *et al.*, 2007). This would also reduce the time taken for manual identification of the markers.

The uncertainties associated with measurements of the motion magnitude were assessed. The largest source of error was the use of a range of gantry angles for measurement of the lateral and vertical motion magnitude. The size of this error was proportional to the magnitude of motion in the orthogonal direction to that being measured. The error was insignificant in the majority of cases, however in cases with large motions the error can become large. For example, errors of 5mm were observed in the case of orthogonal motion of magnitude 40mm.

The size of the error from this source could be estimated, and hence a degree of uncertainty attached to measurements of motion magnitude.

The limited number of projections from which the lateral and vertical motion could be assessed means that little more than a single breathing cycle is included in each range measurement. This could cause uncertainty in the measurement if the breathing cycle observed is not typical or if the motion is irregular. This problem is mitigated by the use of multiple gantry angle ranges (e.g. around -90° and $+90^\circ$) extending the number of breathing cycles over which the motion magnitude is assessed. The longitudinal motion measurement is more robust because the complete sequence of projection images is used. An alternative method to improve the lateral and vertical motion magnitude measurements would be to acquire additional fluoroscopy images along the vertical and lateral directions. However, this would expose the patient to additional x-ray imaging dose and increase the time required for imaging. This departs from the aim of this study, which is to extract additional information from the CBCT projection images that would otherwise be discarded.

In addition to the tumour motion ranges in each direction, it is also possible to determine the principal axes of motion from the CBCT projection images, at least in the transverse plane. This has been demonstrated for the test data and for a patient CBCT image. Information on the direction of the main motion axes is potentially valuable for margin generation in treatment planning. Further studies are in progress using patient data, where major axes of motion will be analysed.

Another problem encountered in this study was that it is not always possible to identify the marker in all projection images. This can be because the marker is outside of the imager's field of view at some gantry angles, or because of other high density structures overlying the image of the marker. The former cause does not occur for markers located close to the centre of rotation (the isocentre), which are usually of the most interest. Shielding of the marker by other objects in the image was found to be a problem for some of the validation images, where metal components in the motor caused opaque shadowing in the projection images. However, this was found to be less problematic in the clinical images, where the high density gold seeds were visible in the vast majority of projections. The effect of missing projection images on the determination of mean marker position was found to be small. Impact on motion range measurement was more significant in the case that projections from the gantry angles required were not available.

4. Conclusion

Intra and inter fraction motion of markers along three orthogonal axes can be extracted from CBCT projection images acquired while the patient is in the treatment position. This has been validated with a marker placed at known positions and moved with known magnitude. Mean marker positions were measured with errors of approximately 1mm or less. Motion ranges were measured with mean error less than 1mm in all directions, although errors of up to 5mm were observed when large magnitude motion was present in an orthogonal direction. Measurement of target position and motion has also been demonstrated to be feasible using patient CBCT projection images. It has also been demonstrated that the principal motion axis in the transverse plane can be derived from the CBCT projections. The intra-fraction motion in particular is additional information which is complementary to the reconstructed volumetric image, and can be extracted without the need for additional fluoroscopic imaging. However, uncertainty in the motion range measurements are greater than could be achieved using additional fluoroscopic imaging.

References

- IEC 1996 Radiotherapy equipment — Coordinates, movements and scales, IEC-61217.
- IEC 1998 Medical electrical equipment — Part 2-1: Particular requirements for the safety of electron accelerators in the range 1 MeV to 50 MeV, IEC 60601-2-1.
- Jaffray D A, Siewerdsen J H, Wong J W and Martinez A A 2002 Flat-panel cone-beam computed tomography for image-guided radiation therapy *Int. J. Radiat. Oncol. Biol. Phys.* **53** 1337-49
- Li T, Schreiber E, Yang Y and Xing L 2006 Motion correction for improved target localization with on-board cone-beam computed tomography *Phys. Med. Biol.* **51** 253-67
- Low D A, Parikh P J, Lu W, Dempsey J F, Wahab S H, Hubenschmidt J P, Nystrom M M, Handoko M and Bradley J D 2005 Novel breathing motion model for radiotherapy *Int. J. Radiat. Oncol. Biol. Phys.* **63** 921-9
- McBain C A, Henry A M, Sykes J, Amer A, Marchant T, Moore C J, Davies J, Stratford J, McCarthy C and Porritt B 2006 X-ray volumetric imaging in image-guided radiotherapy: The new standard in on-treatment imaging *Int. J. Radiat. Oncol. Biol. Phys.* **64** 625
- Oldham M, Letourneau D, Watt L, Hugo G, Yan D, Lockman D, Kim L H, Chen P Y, Martinez A and Wong J W 2005 Cone-beam-CT guided radiation therapy: A model for on-line application *Radiother Oncol* **75** 271-8
- Shirato H, Shimizu S, Kunieda T, Kitamura K, van Herk M, Kagei K, Nishioka T, Hashimoto S, Fujita K, Aoyama H, Tsuchiya K, Kudo K and Miyasaka K 2000 Physical aspects of a real-time tumor-tracking system for gated radiotherapy *Int. J. Radiat. Oncol. Biol. Phys.* **48** 1187-95
- Shirato H, Suzuki K, Sharp G C, Fujita K, Onimaru R, Fujino M, Kato N, Osaka Y, Kinoshita R, Taguchi H, Onodera S and Miyasaka K 2006 Speed and amplitude of lung tumor motion precisely detected in four-dimensional setup and in real-time tumor-tracking radiotherapy *Int. J. Radiat. Oncol. Biol. Phys.* **64** 1229-36
- Smitsmans M H, de Bois J, Sonke J J, Betgen A, Zijp L J, Jaffray D A, Lebesque J V and van Herk M 2005 Automatic prostate localization on cone-beam CT scans for high precision image-guided radiotherapy *Int J Radiat Oncol Biol Phys* **63** 975-84
- Sonke J J, Zijp L, Remeijer P and van Herk M 2005 Respiratory correlated cone beam CT *Med. Phys.* **32** 1176-86
- Sorcini B and Tilikidis A 2006 Clinical application of image-guided radiotherapy, IGRT (on the Varian OBI platform) *Cancer/Radiotherapie* **10** 252-7
- Sykes J R, Whitehurst P and Moore C J 2003 Automatic detection, with confidence, of implanted radiographic seeds at megavoltage energies using an amorphous Silicon imager. In: *Medical Imaging 2003: Visualization, Image-Guided Procedures, and Display*, (San Diego, CA, USA: SPIE) pp 319-29
- Tang X, Sharp G C and Jiang S B 2007 Fluoroscopic tracking of multiple implanted fiducial markers using multiple object tracking *Phys. Med. Biol.* **52** 4081-98